International Journal of Geo-Information

MDPI

Article

Research on Global Off-Road Path Planning Based on Improved A* Algorithm

Zhihong Lv [1,2,3], Li Ni [3], Hongchun Peng [1], Kefa Zhou [2], Dequan Zhao [4], Guangjun Qu [5], Weiting Yuan [1], Yue Gao [4] and Qing Zhang [2,3,*]

[1] School of Marine Technology and Geomatics, Jiangsu Ocean University, Lianyungang 222005, China; 2022220228@jou.edu.cn (Z.L.); penghongchun@jou.edu.cn (H.P.); 2022220253@jou.edu.cn (W.Y.)
[2] Technology and Engineering Center for Space Utilization, Chinese Academy of Sciences, Beijing 100094, China; zhoukf@csu.ac.cn
[3] Institute of Aerospace Information Innovation, Chinese Academy of Sciences, Beijing 100094, China; nili@aircas.ac.cn
[4] School of Information Science and Engineering, Shandong Agricultural University, Tai'an 271000, China; 2022110551@sdau.edu.cn (D.Z.); 2022110547@sdau.edu.cn (Y.G.)
[5] School of Mechanical and Electrical Engineering, Beijing University of Chemical Technology, Beijing 100020, China; 2022210351@mail.buct.edu.cn
* Correspondence: zhangqing@csu.ac.cn

Abstract: In field driving activities, off-road areas usually lack existing paths that can be directly driven on by ground vehicles, but their surface environments can still satisfy the planning and passage requirements of some off-road vehicles. Additionally, the existing path planning methods face limitations in complex field environments characterized by undulating terrains and diverse land cover types. Therefore, this study introduces an improved A* algorithm and an adapted 3D model of real field scenes is constructed. A velocity curve is fitted in the evaluation function to reflect the comprehensive influences of different slopes and land cover types on the traffic speed, and the algorithm not only takes the shortest distance as the basis for selecting extension nodes but also considers the minimum traffic speed. The 8-neighborhood search method of the traditional A* algorithm is improved to a dynamic 14-neighborhood search method, which effectively reduces the number of turning points encountered along the path. In addition, corner thresholds and slope thresholds are incorporated into the algorithm to ensure the accessibility of path planning, and some curves and steep slopes are excluded, thus improving the usability and safety of the path. Experimental results show that this algorithm can carry out global path planning in complex field environments, and the planned path has better passability and a faster speed than those of the existing approaches. Compared with those of the traditional A* algorithm, the path planning results of the improved algorithm reduce the path length by 23.30%; the number of turning points is decreased by 33.16%; and the travel time is decreased by 38.92%. This approach is conducive to the smooth progress of various off-road activities and has certain guiding significance for ensuring the efficient and safe operations of vehicles in field environments.

Keywords: path planning; field environment; environmental modeling; improved A* algorithm

check for updates

Citation: Lv, Z.; Ni, L.; Peng, H.; Zhou, K.; Zhao, D.; Qu, G.; Yuan, W.; Gao, Y.; Zhang, Q. Research on Global Off-Road Path Planning Based on Improved A* Algorithm. *ISPRS Int. J. Geo-Inf.* **2024**, *13*, 362. https://doi.org/10.3390/ijgi13100362

Academic Editors: Wolfgang Kainz and Hartwig H. Hochmair

Received: 24 September 2024
Revised: 14 October 2024
Accepted: 15 October 2024
Published: 16 October 2024

Copyright: © 2024 by the authors. Published by MDPI on behalf of the International Society for Photogrammetry and Remote Sensing. Licensee MDPI, Basel, Switzerland. This article is an open access article distributed under the terms and conditions of the Creative Commons Attribution (CC BY) license (https://creativecommons.org/licenses/by/4.0/).

1. Introduction

With the increasing number of activities, such as ecotourism, geological exploration, and field rescues, the demand for off-road driving has significantly increased, and three-dimensional path planning in complex environmental scenes has gradually become a hot research topic. Conventional path planning algorithms were originally developed for urban environments and are ill-suited for field settings characterized by complex terrains and varied land cover types [1]. In this case, the task of achieving optimal field path planning faces considerable challenges.

Path planning is the process of determining the optimal route from a starting point to a destination through an algorithm. This is a crucial area of research in robot navigation, autonomous driving, and drone navigation. Typically, path planning tasks require identifying the best path from an origin to a destination based on an existing road network topology [2,3]. The off-road environment studied in this paper is different from those examined in previous path planning studies. A field environment contains no known road network, and it is necessary to find points in the given terrain data that can be used as paths. This increases the size of the search area required by the utilized algorithm and increases the difficulty of path planning. In an off-road environment, due to its complexity, to enable a vehicle to quickly and efficiently complete various tasks, it is necessary not only to find the shortest path in the three-dimensional field environment but also to shorten the travel time to the greatest extent possible. Path planning algorithms are generally classified into two main categories: traditional algorithms and intelligent algorithms. Traditional methods encompass the Dijkstra algorithm [4–6], the A* algorithm [7–9], the artificial potential field (APF) method [10,11], and the rapidly-exploring random tree (RRT) algorithm [12–14]. On the other hand, intelligent algorithms comprise the genetic algorithm (GA) [15–17], the ant colony optimization (ACO) algorithm [18,19], the particle swarm optimization (PSO) algorithm [20–22], and neural network algorithms [23,24]. This paper studies the global path planning problem in a field environment with known terrain and land cover conditions. In global path planning tasks, intelligent algorithms, along with the RRT and A* algorithms, are frequently employed [25,26]. These intelligent algorithms are favored for their simplicity in computation, robust performance, and broad applicability [27–29]. However, these methods also have disadvantages, such as slow convergence speeds, low convergence accuracies, and the ease of falling into local optimal solutions when solving high-dimensional path planning problems [30,31]. Though effective, these algorithms have big limitations in extensive and intricate environments. The RRT algorithm is a path planning method that excels in handling complex constraints and offers high search efficiency [32]. However, the quality of the planned paths by this technique is generally average, and this approach can be applied only in special kinds of environments [33,34]. On the contrary, the A* algorithm represents a heuristic search algorithm that excels in graph-based applications. It can rapidly react to alterations in the environment and provides high accuracy with remarkable stability [8]. However, the A* algorithm also has disadvantages, such as a blind search direction, many path turning points, and low search efficiency [35]. However, in relation to this study, the exactness of the path planning results significantly affects the required travel time. The accuracy of an algorithm is more worthy of consideration than its runtime cost. Therefore, this study uses the A* algorithm for path planning and improves upon it.

Recently, several studies have proposed enhancements to the A* algorithm. For instance, Xu et al. [9] refined the algorithm's search method by expanding the traditional 8-neighborhood search to a 48-neighborhood approach. This modification smoothed the generated paths, increased search directions, enhanced path planning efficiency, and reduced the number of turning points. However, this approach is limited to flat paths and does not consider the influence of terrain. Niu et al. [36] improved the heuristic function of the traditional A* algorithm to make the resulting path shorter. However, they did not consider the travel time consumption incurred by the generated path. Hong et al. [37] considered the influence of the slope in the traditional A* algorithm and set different slope thresholds for different vehicles. However, they did not consider whether a vehicle could pass smoothly if the path turned too sharply. This study uses high-precision digital elevation model (DEM) data and aerial drone photography data to perform raster modeling on the experimental area. For path planning problems, most constraints can be derived from the DEM [38]. The A* algorithm has been enhanced for rapid path planning in off-road environments. This enhancement incorporates the effects of slope and land cover type into the algorithm's evaluation function, establishes slope thresholds and turning angle limits,

and excludes areas with obstacles from the search domain. These improvements result in safer planned paths and reduced travel time.

This paper proposes an improved A* algorithm for solving the three-dimensional path planning problem under complex field terrain and land cover types. Most traditional A* algorithms are used in two-dimensional environments, and the improved algorithm expands the application scenario to three-dimensional environments. The evaluation function and search neighborhood of the A* algorithm are improved, and the impacts of different slopes and land cover types on vehicle speed are added to the evaluation function. The path selection process is based not only on the shortest possible distance but also on the determination of the shortest travel speed. The traditional algorithm's 8-neighborhood search method has been upgraded to a dynamic 14-neighborhood search, significantly reducing the count of turning points along the path. Additionally, corner and slope thresholds have been integrated into the enhanced algorithm to ensure path accessibility. Ultimately, this process generates the optimal three-dimensional path for field applications.

2. Data and Environment Modeling

2.1. Research Area and Data

To ensure the representativeness of the conducted experiment, Emin County of the Tacheng District, Xinjiang Uygur Autonomous Region, is selected as the study site. The study area features intricate terrain, varied landforms, and distinct elevation gradients, offering substantial data backing for the creation of a test environment model.

Numerous public datasets, including SRTM1, GSDEM-30, and AW3D30 DEM, feature a resolution of 30 m. However, in off-road path planning tasks, vehicles are regarded as particles for path planning, and fine-grained DEM data are required to provide data support for experiments. In actual off-road environments, terrain changes affect the vehicle's ability to pass, so fine-grained DEM data can better reflect real-world conditions. These data provide more detailed terrain information, including slopes, obstacles, and surface cover types, which are key factors affecting vehicle driving. In addition, detailed terrain information helps the algorithm avoid potential collision risks when planning the path, thereby improving the safety and effectiveness of the path. This study uses a DJI Matrice 350 RTK drone (DJI, Shenzhen, China) equipped with a Zenmuse P1 camera (DJI, Shenzhen, China) to obtain DEM data for the study area with a resolution of 0.025 m. Since high-resolution data increase the complexity and time required for calculations and cause information redundancy, the obtained DEM data are resampled to obtain DEM data with a 0.5-m resolution. The data include 800 × 500 cells, which are equivalent to an actual area of approximately 0.1 km^2. Figure 1 shows the specific location of the experimental area, as well as the visible light images and DEM data obtained using a drone.

2.2. Environmental Modeling

2.2.1. Terrain Modeling

In a three-dimensional environment, terrain gradient information is a critical factor influencing path planning tasks. By analyzing the gradient characteristics derived from the DEM, practical and impractical areas are identified to assess the suitability of paths for various off-road vehicles.

In this research, solely the slope of the DEM is computed, while the slope direction is not considered. It is presumed that the projection region of the car is a grid cell. The values of the central pixel and its eight adjacent pixels determine the horizontal and vertical increments. These adjacent pixels are identified by letters a to i, where e represents the pixel for which the slope is currently being calculated, as shown in Figure 2. Utilizing this information, Equations (1) and (2) calculate the slope in the X orientation $Slope_X$ and the slope in the Y orientation $Slope_Y$, respectively.

$$Slope_X = \frac{(c + 2f + i) - (a + 2d + g)}{8 * CellSize} \quad (1)$$

$$Slope_Y = \frac{(g + 2h + i) - (a + 2b + c)}{8 * CellSize} \quad (2)$$

where $CellSize$ represents the spacing of the grid DEM.

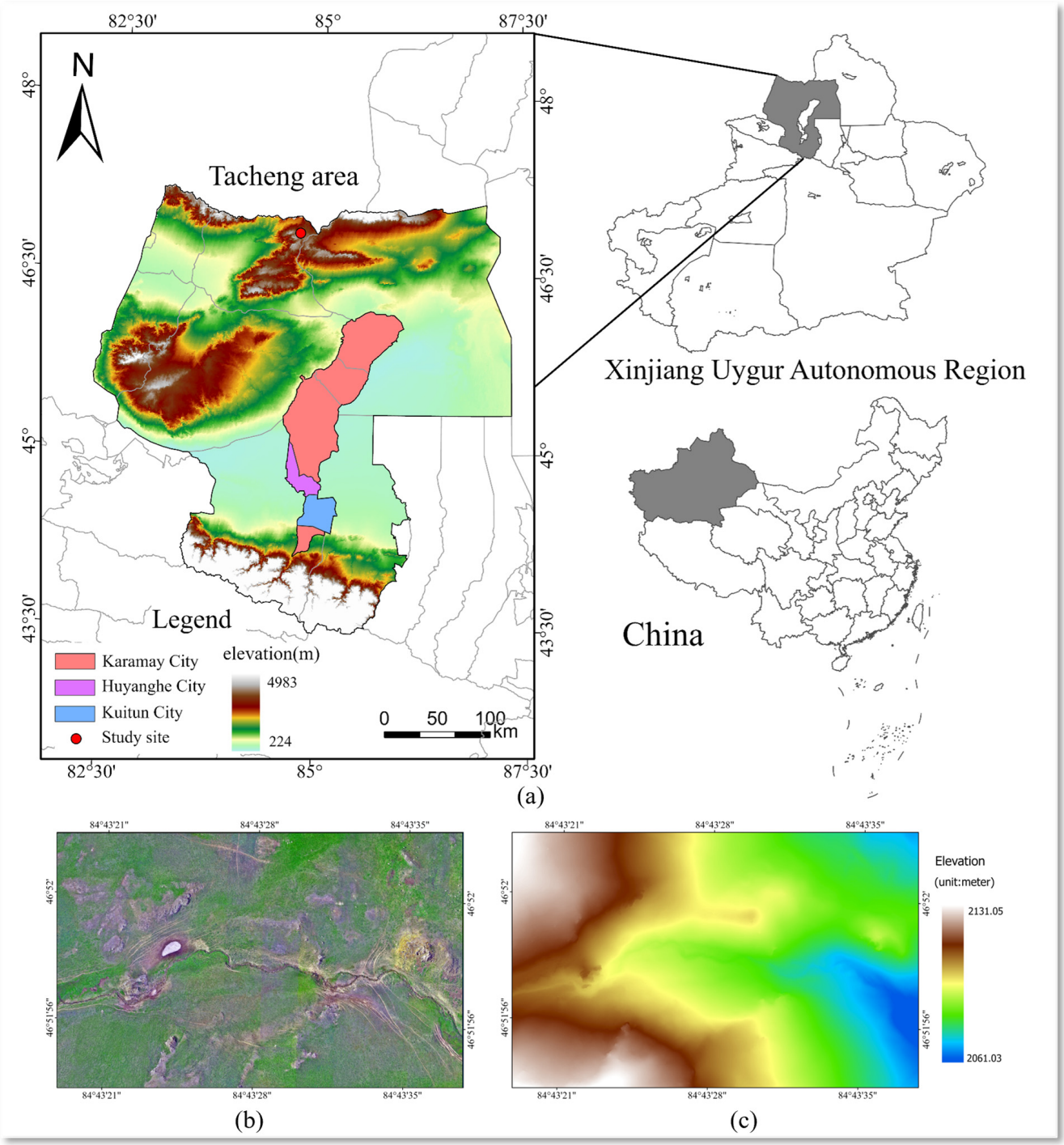


Figure 1. Overview of the study area. (**a**) Geographic location of the study area, (**b**) visible light image of the study area, and (**c**) DEM image of the study area.

The slope is calculated as the rate of surface change from the center cell to each adjacent cell in the horizontal and vertical directions. The calculation formula is shown below.

$$Slope = arctan\sqrt{{Slope_X}^2 + {Slope_Y}^2} \quad (3)$$

The described method is employed to transform the study area's DEM into a slope map, as shown in Figure 3a. Referring to the dynamic index of a car [39], the maximum climbing gradient i_{max} of the car usually refers to the climbing ability of the car in gear I. The i_{max} of a general vehicle is approximately 16.7°. Off-road wheeled vehicles typically navigate on poor roads or in areas without any roads, so i_{max} is relatively large (approximately 31°). To ensure the safe passage of the vehicle, the uphill and downhill thresholds in this experiment are set to 30°. The areas in the slope map exceeding 30° are extracted and set as obstacles. The extraction outcomes are presented in Figure 3b.

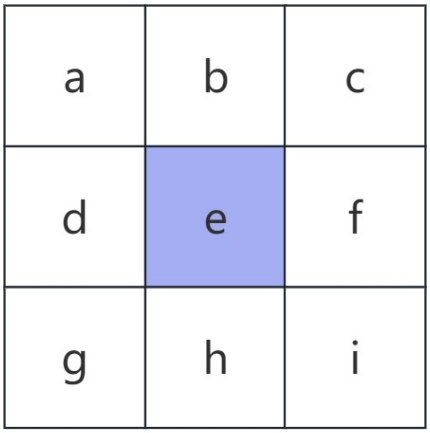


Figure 2. Central 3 × 3 cell grid.

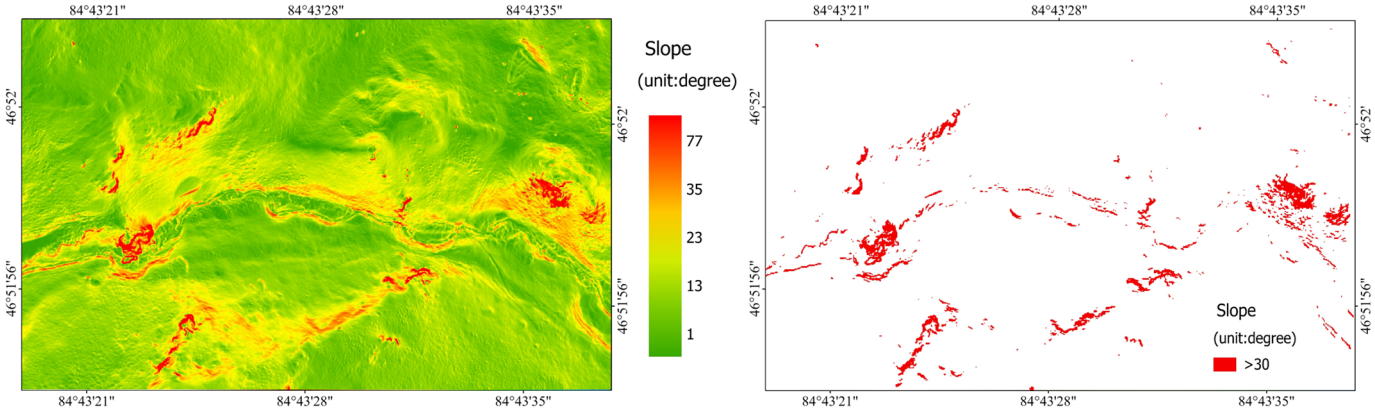


Figure 3. Slope map of the study area. (**a**) Slope map of the study area and (**b**) slopes of the areas exceeding 30°.

2.2.2. Land Cover Type Modeling

Different land cover types have different effects on the vehicle speed, so high-precision unmanned aerial vehicle (UAV) photography data are subjected to supervised classification operations, and the support vector machine method is used to obtain four land cover types—grassland, water areas, wasteland, and saline—alkali land—from the image data. The kappa coefficient is 0.94. The outcomes are presented in Figure 4.

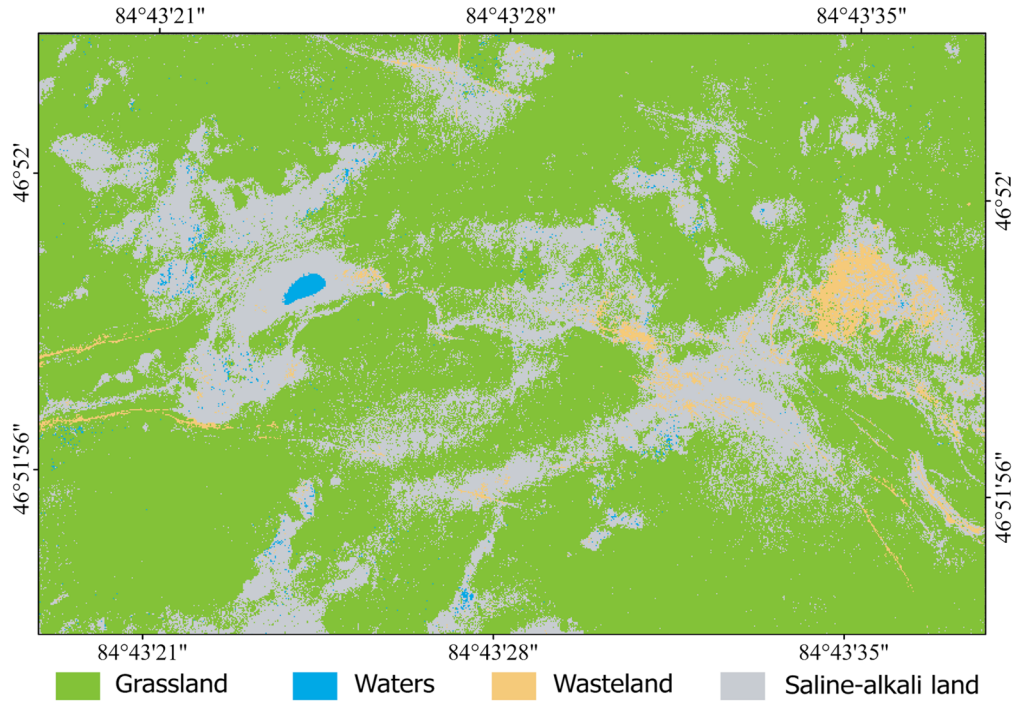


Figure 4. Land cover type map of the study area.

2.2.3. Field Environment Modeling

After modeling the various attribute layers, they need to be overlaid for analysis purposes to complete the field environment modeling task. The traditional method is to map the above data into grid coordinates to establish an environmental model [40]. This method offers advantages such as a straightforward data structure, ease of performing spatial analysis, and the integration of multilevel spatial data. However, the resulting map remains a conventional single-layer map. Therefore, this research adopts an improved method [41] to enhance the simple data structure and construct a multilevel feature map for storing land cover information, slope obstacles, and 3D coordinate information, as shown in Figure 5. This approach effectively preserves the environmental trait data and enhances the maintainability of the cost map. The overlay algorithm first employs the DEM data as the base layer to display the terrain information for the experiment. Next, the land use data are overlaid on top of the DEM layer, utilizing specific color mappings to visualize different land cover types. Finally, the obstacle layer is superimposed at the corresponding positions based on precise coordinate information, thereby completing the modeling process of the real-world 3D environment. The consequent map is illustrated in Figure 6.

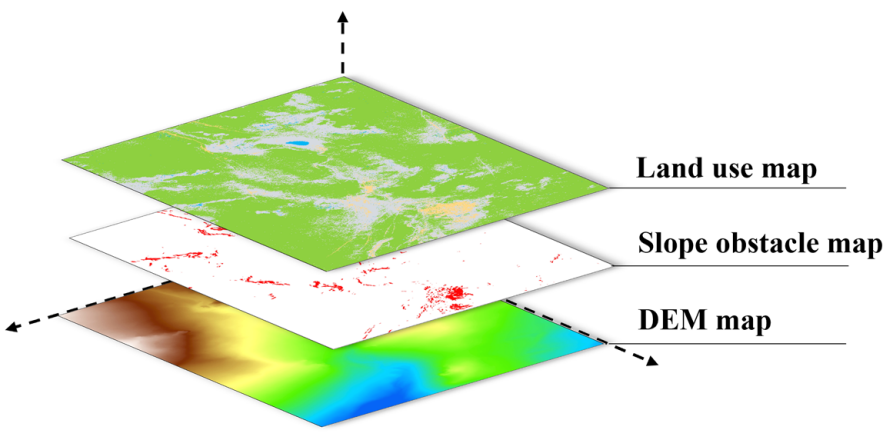


Figure 5. Layer overlay.

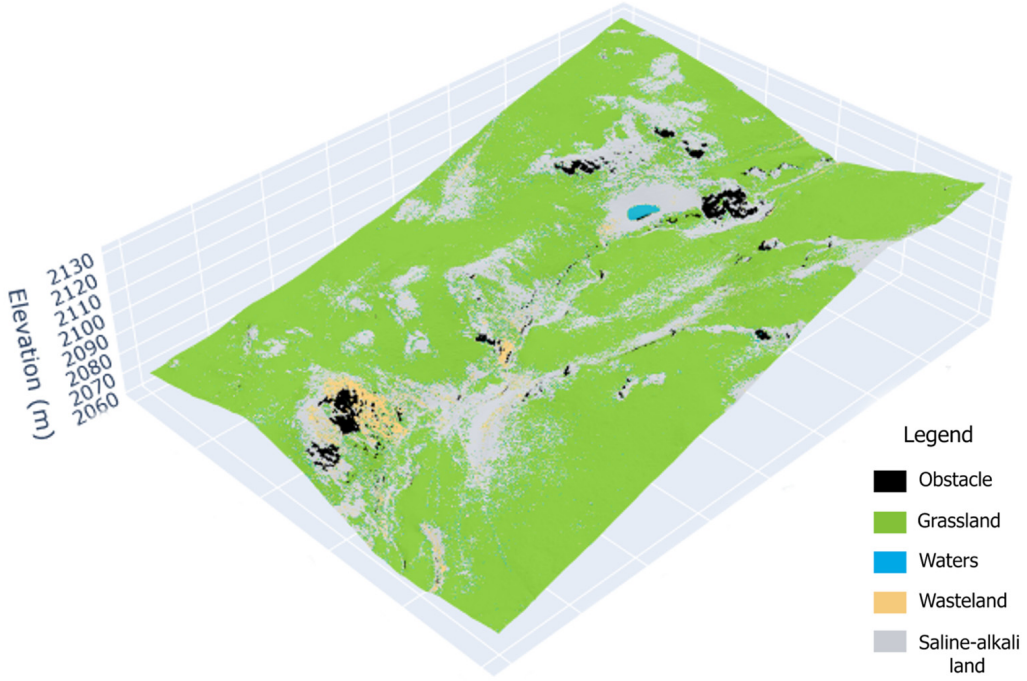


Figure 6. Real-world 3D environment modeling results.

2.2.4. Grid Cost Assignment

In a field environment, the main factors affecting passability are the types of surface features that are present and the terrain slope. Taking an off-road vehicle as an example, field experiments were conducted to measure the vehicle's speed under different slopes and terrain types. The Aowei Interactive Map software 10.1.3 was used to record the vehicle's speed under the same power conditions across different slopes and land cover types. Given the difficulty of maintaining constant vehicle power, the experiment involved observing and controlling the vehicle's RPM, keeping it as stable as possible around a fixed value to idealize this process. Ultimately, the experiment determined the rate of speed reduction under various conditions. Based on its driving characteristics in different surface environments, the driving speeds produced for four representative types of features, namely, grassland, wasteland, saline—alkali land, and water, and corresponding to three typical slope values are given [42]. As shown in Table 1, the maximum passable slope of the vehicle varies under different surface conditions. Flat land, that is, terrain with a slope of 0°, generally has the maximum passable speed. While ensuring the safety of field driving, the speed should be appropriately reduced when moving downhill. For simplicity, the same speed as that of going uphill is used. According to general experience, 10° is the middle value with the highest slope value frequency, so it is taken as a typical slope value.

Table 1. Speed and resistance of traffic corresponding to the types of terrain and different slopes.

Type of Landform	0° Passing Speed	0° Traffic Resistance	10° Passing Speed	10° Traffic Resistance	Maximum Passing Angle
Field road	30 km/h	1	15 km/h	2	30°
Grassland	12 km/h	2.5	4 km/h	7.5	20°
Wasteland	20 km/h	1.5	10 km/h	3	25°
Salt-alkali land	16 km/h	1.875	8 km/h	3.75	25°
Waters	0 km/h	∞	0 km/h	∞	0°

In terms of landform types, if a road is present in the field, the passability of the field road is optimal. Let $V_0 = 30$ km/h denote the benchmark speed, and let the corresponding

resistance value $r_0 = 1.0$. The speeds for other landform types are determined via field tests and empirical estimates based on flat land as a reference. For example, considering that wasteland is mainly composed of small gravel, the ground is relatively stable, and its speed is faster; saline—alkali land is slightly weaker than wasteland; grassland has a certain sand fixation effect, so it also has a certain degree of passability; and water areas are set as impassable.

The existing studies generally considered the construction of the travel cost function in a relatively simple manner. Based on general experience, this study believes that the relationship between vehicle speed, terrain, and slope is a quadratic nonlinear function, not the simple linear relationship given in the general literature. Therefore, based on the three point values shown in Table 1, the function fitting method is used to obtain the corresponding speed and travel resistance expressions under arbitrary slope conditions for different terrain types.

The expressions $V(T,\theta)$ and $r(T,\theta)$ for calculating vehicle speed and resistance levels, respectively, under different surface features and slope environments are as follows:

$$V(T,\theta) = \begin{cases} 66.09 \times (tan\theta)^2 - 57.02 \times tan\theta + 12, \ T = grassland \\ 47.67 \times (tan\theta)^2 - 65.12 \times tan\theta + 20, \ T = wasteland \\ 38.13 \times (tan\theta)^2 - 52.09 \times tan\theta + 16, \ T = saline - alkali\ land \\ 0, \ T = waters \end{cases} \tag{4}$$

$$r(T,\theta) = \begin{cases} \frac{V_0}{V(T,\theta)}, \left(T \neq waters, V_0 = \frac{30\ \mathrm{km}}{h}\right) \\ \infty, \ (T = waters) \end{cases} \tag{5}$$

where T represents the different land types, θ is the angle value for expressing the slope, and $tan\theta$ is the slope value expressed as a percentage. Figure 7 shows the quadratic curves corresponding to the four types of land features, and the horizontal axis is the slope value expressed as a percentage. According to the above functional relationship, the traffic speed of off-road vehicles on the surface and the arbitrary slopes of distinct feature types can be computed, and the accuracy of traffic cost estimation can be improved.

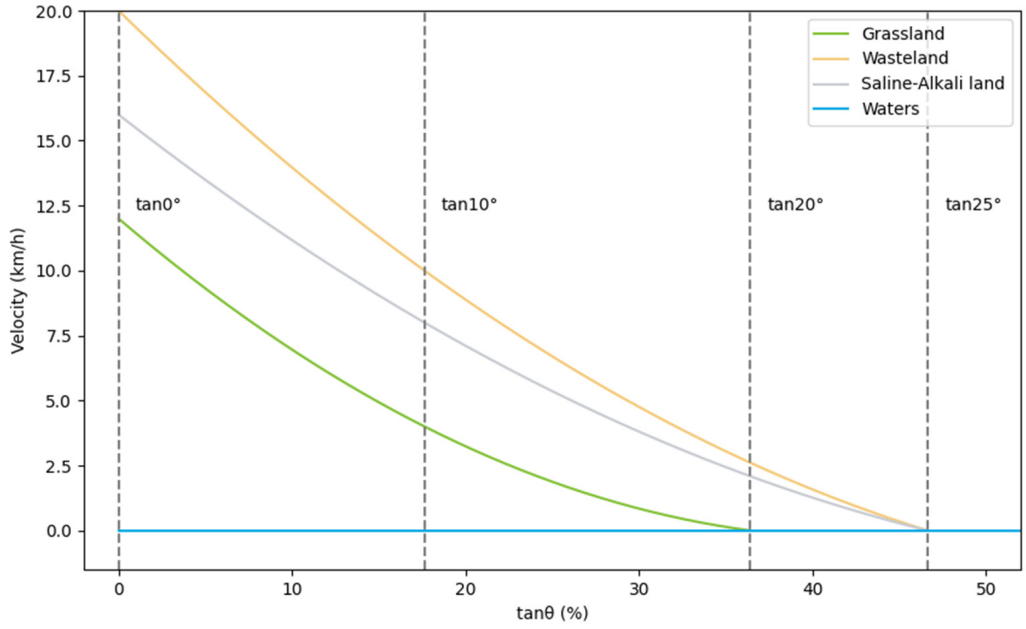


Figure 7. Slope and speed curves produced for different types of terrain.

Through the above method, the slope and land cover information of each grid in the study area can be transformed, and the terrain data can be mapped as corresponding passage speed values via speed curve fitting. Specifically, the slope and land cover type

jointly determine the vehicle's speed within each grid. The transformed grid stores passage speed information based on different terrain conditions, effectively reflecting the vehicle's passability in complex terrains. This approach of converting terrain and land cover data into speed values not only improves the accuracy of the path planning algorithm's travel time prediction but also optimizes path selection, significantly enhancing the algorithm's practicality and reliability in complex off-road environments.

3. Path Planning Algorithm

3.1. Traditional A Algorithm*

The A* algorithm is a widely used heuristic search method for path planning. It determines the shortest route from a starting point to an endpoint within a finite set of traversable paths. The heuristic distance cost function is defined as follows [43,44]:

$$F(n) = G(n) + H(n) \tag{6}$$

$$G(n) = G' + \sqrt{(x_n - x_{n-1})^2 + (y_n - y_{n-1})^2} \tag{7}$$

$$H(n) = \sqrt{(x_z - x_n)^2 + (y_z - y_n)^2} \tag{8}$$

where $F(n)$ represents the total estimated cost from the start point to the goal point. $G(n)$ denotes the actual cost from the start node to the current node n, while $H(n)$ is the estimated cost from the current node n to the goal node. G' signifies the original cost from the previous node to the initial node. The coordinates (x_n, y_n) indicate the current node, (x_{n-1}, y_{n-1}) represent the parent node, and (x_z, y_z) denote the goal node.

3.2. Improved A Algorithm*

3.2.1. Improved Evaluation Function

In a field environment, complex terrain is an important factor that affects vehicle traffic. To make the obtained path planning results safer and more efficient, the traditional A* algorithm is improved. The influences of the slope and land cover type are added to the evaluation function so that the improved A* algorithm selects areas with gentle slopes that are less affected by land types. In addition, corner and slope thresholds are added to the A* algorithm. When the corner of the determined path is too large or exceeds the slope threshold, it is considered impassable. Simultaneously, obstacle parameters are added to ensure that the generated path can effectively avoid obstacles.

The improved evaluation function parameters $G(n)$ and $H(n)$ are as follows:

$$G(n) = G' + V(T,\theta)_{min}\sqrt{(x_n - x_{n-1})^2 + (y_n - y_{n-1})^2} \tag{9}$$

$$H(n) = V(T,\theta)_{min}\sqrt{(x_z - x_n)^2 + (y_z - y_n)^2} \tag{10}$$

where G' represents the original cost from the previous node to the initial node and $V(T,\theta)_{min}$ represents the minimum speed, which can be calculated using Equation (4). (x_n, y_n) is the current node, (x_{n-1}, y_{n-1}) is the parent node, and (x_z, y_z) is the target node.

In path planning for vehicles driving in off-road environments, improving the smoothness of the path is of critical importance. A smooth path can significantly enhance driving safety by reducing sharp turns and frequent direction changes, thereby lowering the risk of vehicle loss of control or rollover, especially in rugged terrains and complex obstacle environments. To address this issue, a path smoothing function is incorporated into the evaluation function of the improved algorithm to ensure the safety and practicality of the path planning. As shown in Figure 8, (a) represents the path planning results without smoothing, and (b) represents the path planning results after applying the path smoothing function. It can be observed from the figure that the smoothed path has significant advantages compared to the original path.

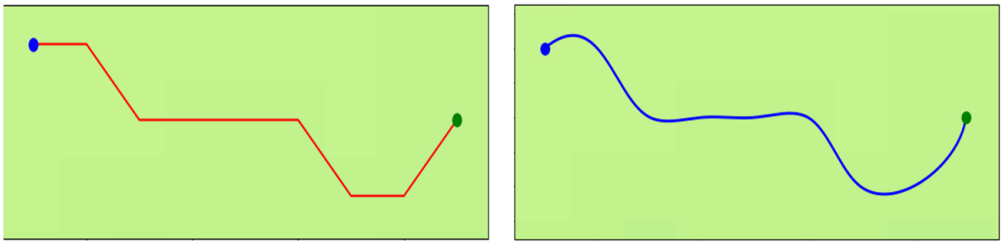


Figure 8. Implementation of path smoothing function. (**a**) Traditional path planning results; (**b**) Path planning results after improving the path smoothing function.

3.2.2. Search Neighborhood Improvements

The conventional A* algorithm examines eight neighboring nodes around the current node. Building on the original search method, the search directions have been extended to encompass 24 directions, as shown in Figure 9, which increases the freedom of the search and reduces the count of encountered turning points. However, the 24-direction search method increases the count of search nodes and reduces the search effectiveness. Therefore, the expanded 24-neighborhood search is improved to a dynamic 14-neighborhood search, which increases the search effectiveness and reduces the count of search nodes. The retained node is selected by determining the angle between the positive direction of the vertical line of the current node and the direction of the line connecting the current node and the end point. Figure 10 shows the search method. Table 2 provides the search rules.

i	j	k	l	m
s	a	b	c	n
w	h	Current Node	d	o
v	g	f	e	p
u	t	s	r	q

Figure 9. 24-node neighborhood graph.

Table 2. Dynamic 14-neighborhood search rules.

Clamping Angle	Reserved Nodes
[0, 22.5°) ∪ [337.5°, 360°)	a, b, c, d, h, i, j, k, l, m, n, o, w, s
[22.5°, 67.5°)	a, b, c, d, e, i, j, k, l, m, n, o, p, q
[67.5°, 112.5°)	b, c, d, e, f, k, l, m, n, o, p, q, r, s
[112.5°, 157.5°)	c, d, e, f, g, m, n, o, p, q, r, s, t, u
[157.5°, 202.5°)	d, e, f, g, h, o, p, q, r, s, t, u, v, w
[202.5°, 247.5°)	e, f, g, h, a, q, r, s, t, u, v, w, s, i
[247.5°, 292.5°)	f, g, h, a, b, s, t, u, v, w, s, i, j, k
[292.5°, 337.5°)	g, h, a, b, c, u, v, w, s, i, j, k, l, m

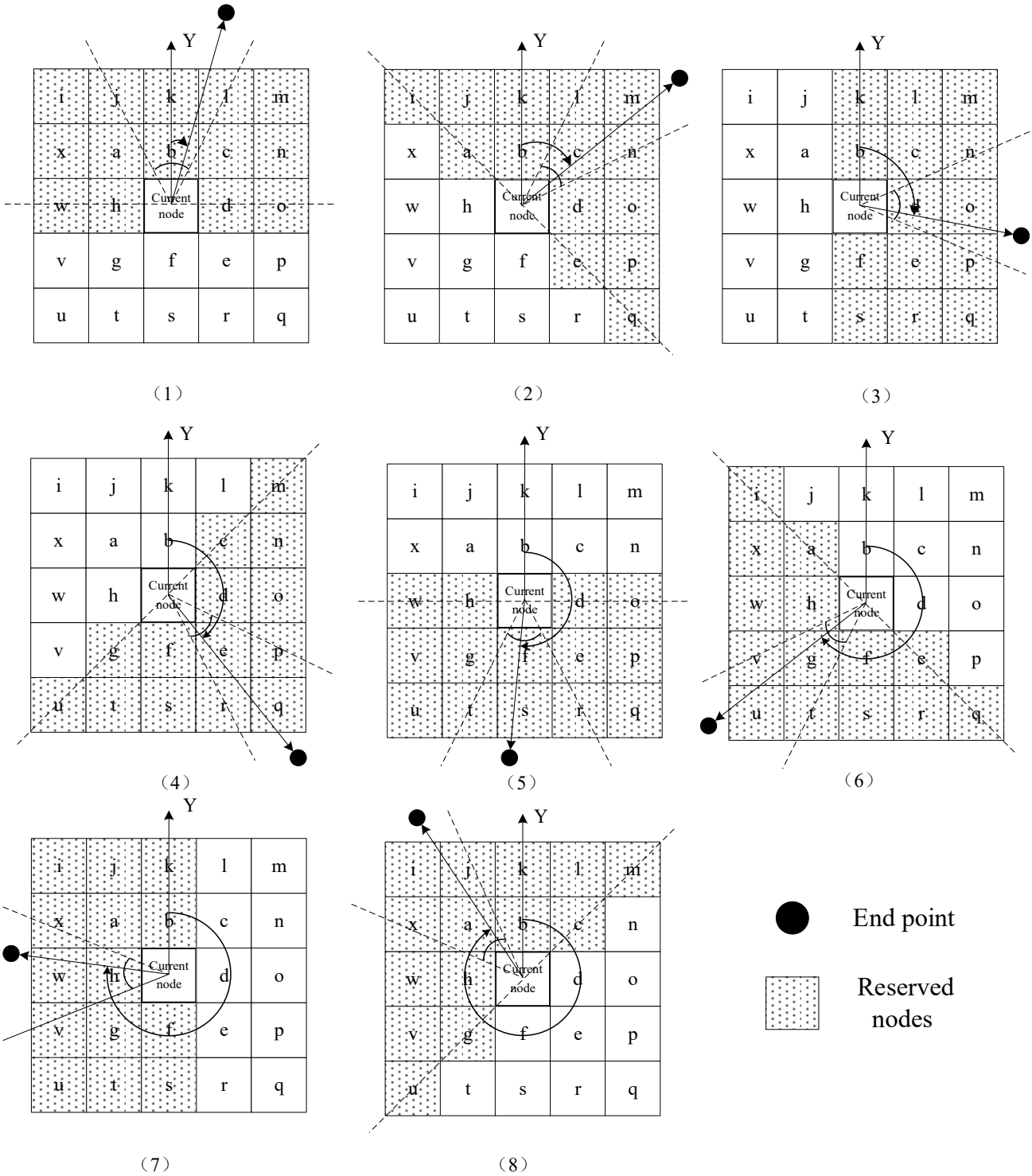


Figure 10. Dynamic 14-neighborhood method: (**1**–**8**) are the field selection diagrams under eight different angles.

The traditional A* algorithm does not consider the volume of the vehicle used, which can lead to situations where the path diagonally crosses obstacle vertices. In practical applications, crossing the obstacle vertex diagonally will cause a collision and create safety issues. Therefore, this study improved the search algorithm and set each obstacle grid and the 24 nodes around it as a no-entry area. The algorithm will skip these grids during the search calculation to ensure the safety of the constructed path. As illustrated in Figure 11, panel (a) presents the results of traditional obstacle avoidance path planning, while panel

(b) displays the outcomes of the improved obstacle avoidance path planning. The figure clearly demonstrates that the improved obstacle avoidance functionality effectively guides the path away from obstacles, thereby ensuring the safety of the planned route.

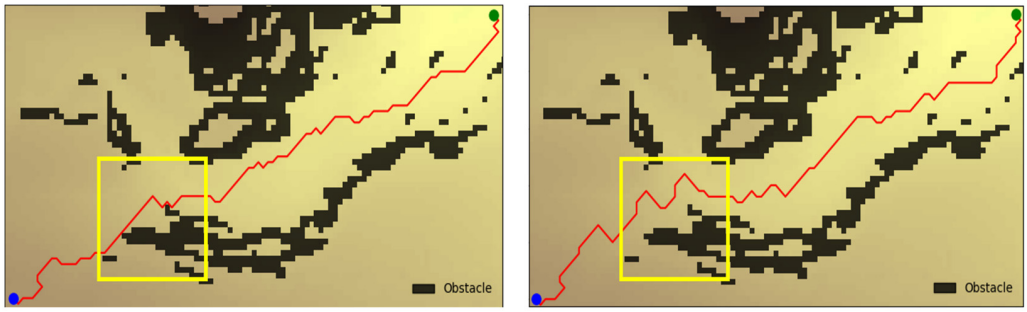


Figure 11. Obstacle avoidance function implementation. (**a**) The path planning result of the traditional A* algorithm; (**b**) The path planning result of the improved A* algorithm.

3.2.3. Improving the Process of the A* Algorithm

By improving the evaluation function and search neighborhood of the traditional A* algorithm, the issues of excessive turning points in the path and insufficient considerations have been addressed. The specific algorithmic flow is shown in Figure 12.

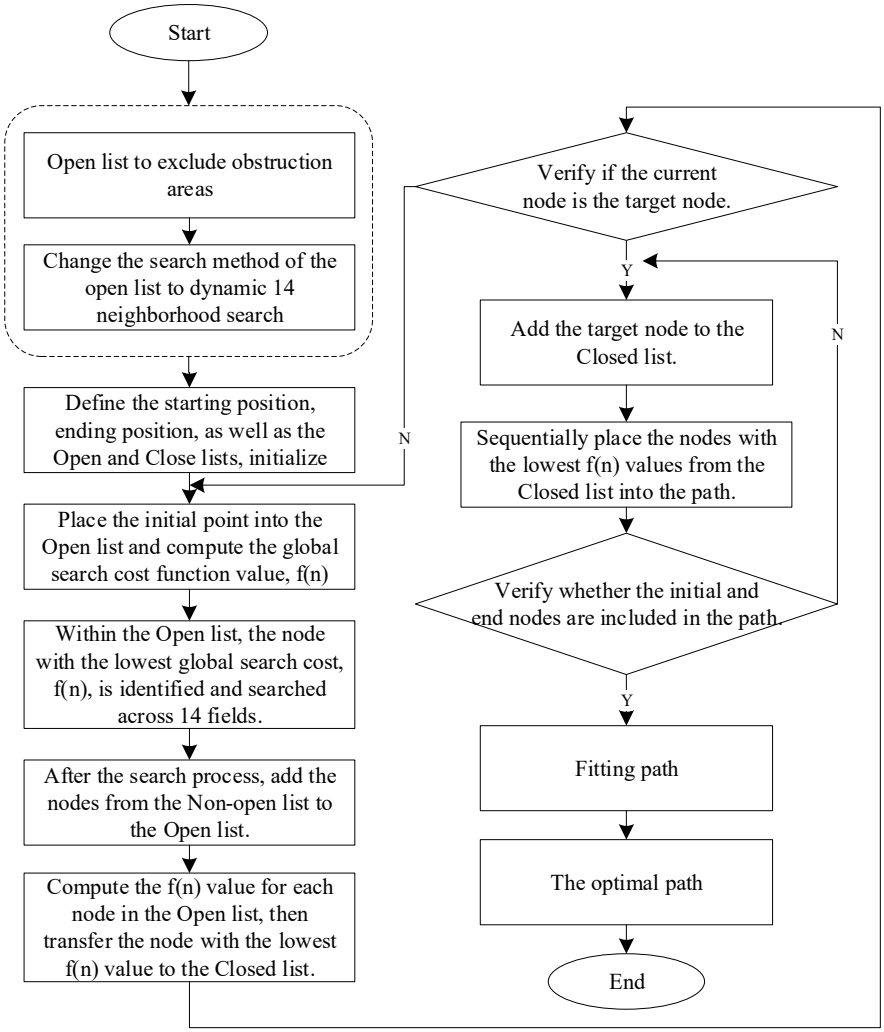


Figure 12. Flowchart of the improved A* algorithm.

4. Experiments and Results

To test the performance of the improved A* algorithm, two travel conditions, namely, the shortest travel distance and shortest travel time, are considered. The applicability of the improved algorithm is verified by comparing the path planning results from various algorithms within the same field environment.

This experiment is implemented using Python 3.9 on a device with a 4.90-GHz CPU and 16.00 GB of RAM, and a path planning simulation test is completed.

4.1. Shortest Path Planning under the Influence of Slope

This section discusses the impact of considering the slope factor (excluding land cover factors) on the shortest path planning result of the A* algorithm. In Figure 13, two path planning results of three different algorithms (the traditional A* algorithm, the 24-neighborhood A* algorithm, and the improved A* algorithm) are given. The traditional A* algorithm also includes terrain judgment conditions; otherwise, a slanted line or straight line would be observed from the initial point to the destination. The blue point in the figure represents the initial, and the green point represents the destination. According to Table 3, in field path 1 the improved A* algorithm reduces the path length by 14.52% and the number of turning points by 50.49% in comparison to the traditional A* algorithm; in field path 2 the improved A* algorithm reduces the path length by 7.32% and the number of turning points by 45.90% in comparison to the traditional A* algorithm. The analysis of the results from three path planning algorithms applied to two different field paths shows that, although the 24-neighborhood A* algorithm improves path length and the number of turning points compared to the traditional A* algorithm, its run time is several times longer. The improved A* algorithm produces shorter paths than the traditional A* algorithm, with an average reduction of 10.92% in path length and a 48.20% reduction in the number of turning points. However, the run time increases by 48.96%.

Table 3. The shortest path planning results obtained under the influence of terrain.

	Algorithm	Path Length (m)	Number of Turning Points	Run Time (s)
Path 1	Traditional A* algorithm	387.19	612	77.48
	24 search neighborhood A* algorithm	372.46	336	358.54
	Improved algorithm	330.96	303	120.10
Path 2	Traditional A* algorithm	426.81	719	68.07
	24 search neighborhood A* algorithm	436.30	421	311.47
	Improved algorithm	395.58	389	97.28

4.2. Planning the Path with the Shortest Travel Time under the Influence of Land Cover

This section describes how land cover factors (excluding the slope) affect the shortest path planning results of the A* algorithm. Figure 14 shows the planning results obtained for three different paths in the field using two algorithms (the traditional A* algorithm, the 24-neighborhood A* algorithm, and the improved A* algorithm). The blue dot represents the starting point, and the green dot represents the endpoint.

As indicated in Table 4, for field path 1, the improved A* algorithm reduces the path length by 2.92%, the count of turning points by 39.26%, and travel time by 4.48% compared to the traditional A* algorithm. For field path 2, the improved algorithm decreases the path length by 9.85%, the count of turning points by 51.55%, and travel time by 3.41%. By combining the two results, it can be seen that in terms of the impact of land cover on the resulting travel time and path length, the improved A* algorithm has a small advantage. The 24-neighborhood A* algorithm performs the best in terms of travel time, but it has the longest running time.

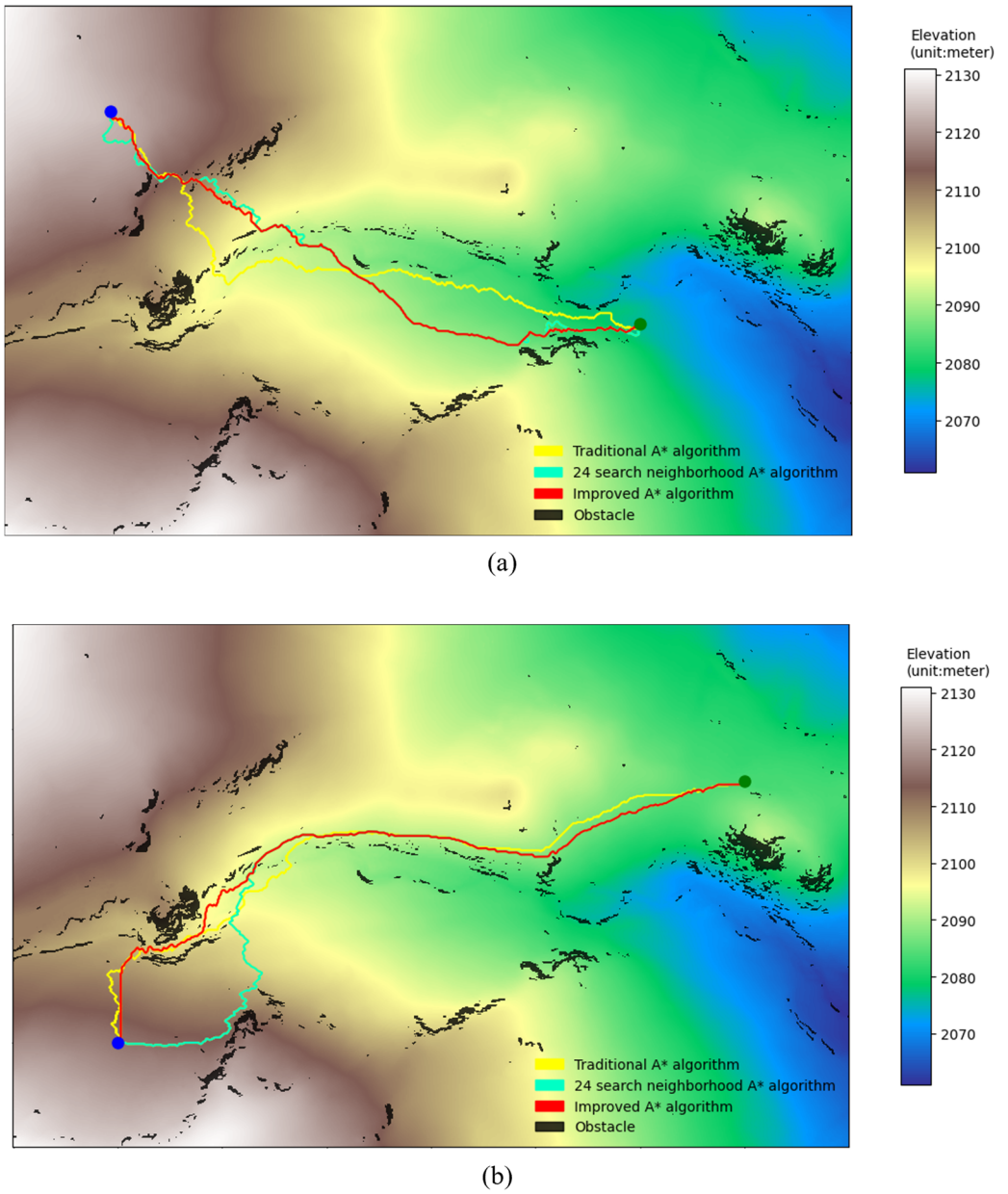
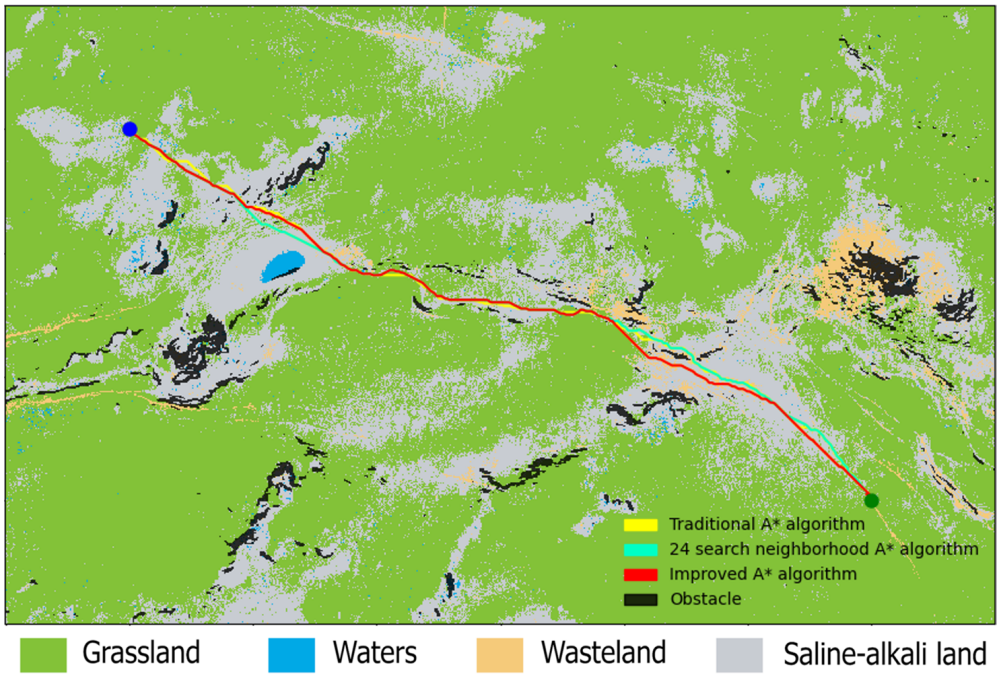


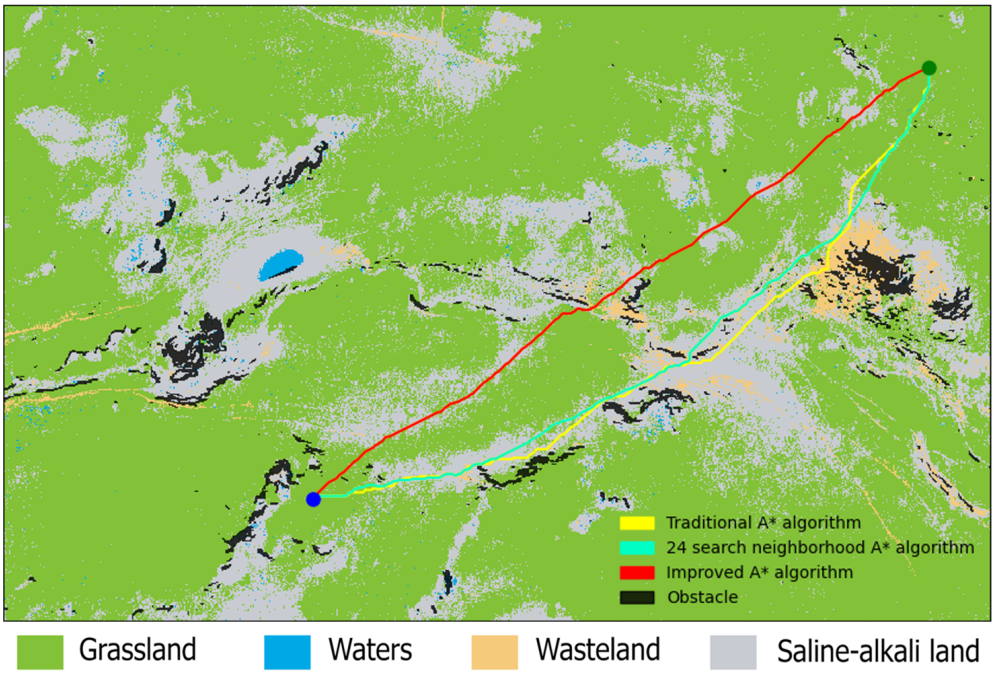
Figure 13. Shortest path planning results obtained under the influence of terrain. (**a**) Comparison experimental results of the traditional A* algorithm, the 24-neighborhood A* algorithm, and the improved A* Algorithm for Path 1; (**b**) Comparison experimental results of the traditional A* algorithm, 24-neighborhood A* algorithm, and the improved A* Algorithm for Path 2.

Table 4. Comparison of time-shortest path planning results under the influence of land cover.

	Algorithm	Path Length (m)	Number of Turning Points	Travel Time (s)	Run Time (s)
Path 1	Traditional A* algorithm	367.70	619	165.23	44.55
	24 search neighborhood A* algorithm	357.66	389	154.52	199.10
	Improved algorithm	356.96	376	157.83	88.89
Path 2	Traditional A* algorithm	346.92	582	159.76	50.23
	24 search neighborhood A* algorithm	331.59	331	149.78	221.49
	Improved algorithm	312.75	282	154.32	58.65



(a)



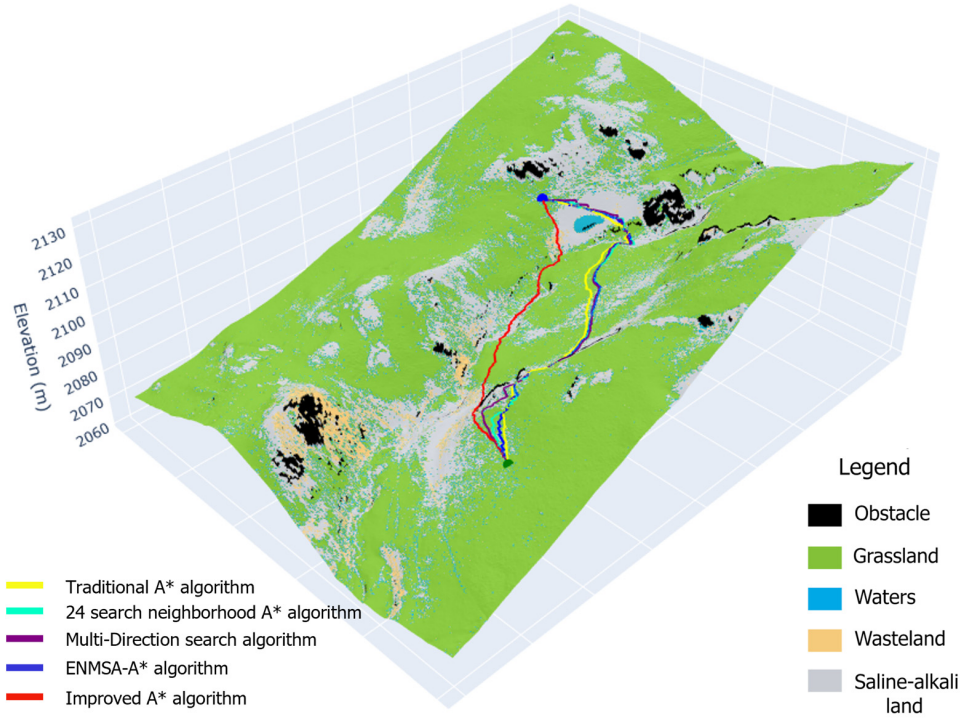
(b)

Figure 14. The paths with the shortest travel times planned under the influence of land cover. (**a**) Comparison experimental results of the traditional A* algorithm, the 24-neighborhood A* algorithm, and the improved A* Algorithm for Path 1; (**b**) Comparison experimental results of the traditional A* algorithm, 24-neighborhood A* algorithm, and the improved A* Algorithm for Path 2.

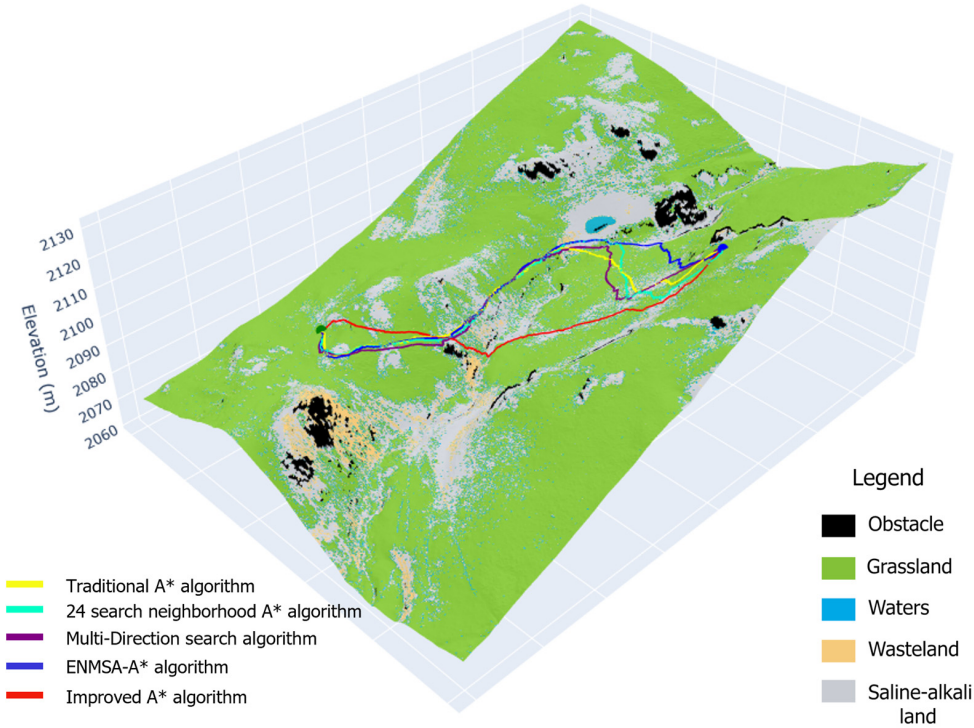
4.3. Optimal Path Planning Results Obtained under a Comprehensive Influence

This section discusses the path planning results produced by different algorithms that consider the influences of the slope and land cover type at the same time. Figure 15 shows the planning results obtained by five algorithms (the traditional A* algorithm, the 24 search neighborhood A* algorithm, the multi-direction search algorithm [45], the ENMSA-A*

algorithm [46], and the improved A* algorithm) for two different field paths, where blue depicts the starting point and green depicts the endpoint.



(a)



(b)

Figure 15. Optimal path planning results under the combined influence of terrain and land cover factors. (**a**) Comparative experimental results of five different algorithms on Path 1; (**b**) Comparative experimental results of five different algorithms on Path 2.

As shown in Table 5, different algorithms have their own advantages and disadvantages in various aspects. The multi-directional search A* algorithm performs best in optimizing path turning points but has a slower execution speed. In contrast, the improved A* algorithm proposed in this study excels in path length and travel time; however, its results in terms of the number of turning points and execution time are inferior to those of other algorithms. Combining the analyses of both paths, the improved algorithm reduces the path length by 23.30%, the number of turning points by 33.16%, and the travel time by 38.92% compared to the traditional A* algorithm.

Table 5. Optimal path planning results obtained under a comprehensive influence.

	Algorithm	Path Length (m)	Number of Turning Points	Travel Time (s)	Run Time (s)
Path 1	Traditional A* algorithm	305.49	507	218.75	61.14
	24 search neighborhood A* algorithm	312.25	352	221.62	260.23
	Multi-Direction search algorithm	318.56	219	210.08	330.01
	ENMSA-A* algorithm	308.09	361	208.63	148.36
	Improved algorithm	244.43	336	140.47	180.59
Path 2	Traditional A* algorithm	365.04	617	309.05	58.50
	24 search neighborhood A* algorithm	405.39	438	326.53	291.95
	Multi-Direction search algorithm	388.86	267	310.57	462.55
	ENMSA-A* algorithm	371.92	468	307.92	161.46
	Improved algorithm	267.94	416	179.12	207.35

5. Discussion

This experiment addresses the path planning problem in wild environments and improves the evaluation function and search method of the traditional A* algorithm. In the A* algorithm, a combined judgment of terrain and land cover type has been added, thus enabling the algorithm to find a shorter path with a shorter travel time in a complex environment; the traditional 8-direction search method is improved to a dynamically selected 14-direction search method, which can reduce the number of turning points encountered along the path, and obstacle avoidance and corner restriction functions are added to the algorithm. The algorithm can provide safe and efficient path planning results that are suitable for vehicle traffic in complex field environments.

In shortest path planning experiments conducted under the influence of the slope, only the influence of terrain on the results of different algorithms is considered. A slope judgment term is included in the A* algorithm. Three different search methods, the traditional 8-neighborhood method, the 24-neighborhood A* algorithm, and the improved dynamic 14-neighborhood method, are used for the experiments. Due to the use of different search methods, the obtained experimental results are also different. The traditional 8-neighborhood search method and the 24-neighborhood A* algorithm involves processing points far from the target node when searching for the optimal path. The improved dynamic 14-neighborhood search method limits the search orientation of the path so that search node always moves toward the target point and mitigates the issue of many turning points. Comparison of the results is shown in Figure 16. The improved dynamic 14-neighborhood search method can effectively shorten the lengths of the formed paths and reduce the numbers of path turning points for two different field paths, thereby improving the safety of vehicle driving.

In the shortest path planning experiments conducted under the influence of land cover, a travel time judgment term is added to the A* algorithm. Since terrain conditions are not considered, only the influence of the land cover type on the speed of vehicle travel is considered. The experiments are conducted using different search methods. The outcomes of the experiment are illustrated in Figure 17. The improved algorithm provides small path length and travel time improvements over those of the traditional 8-neighborhood search method and greatly optimizes the number of turning points. The improved algorithm has

a significant improvement in running time compared to the 24-neighborhood algorithm. The above two experiments prove that the improved dynamic 14-neighborhood search method yields good path distance and travel time improvements over the traditional 8-neighborhood search, and the number of turning points is also significantly reduced.

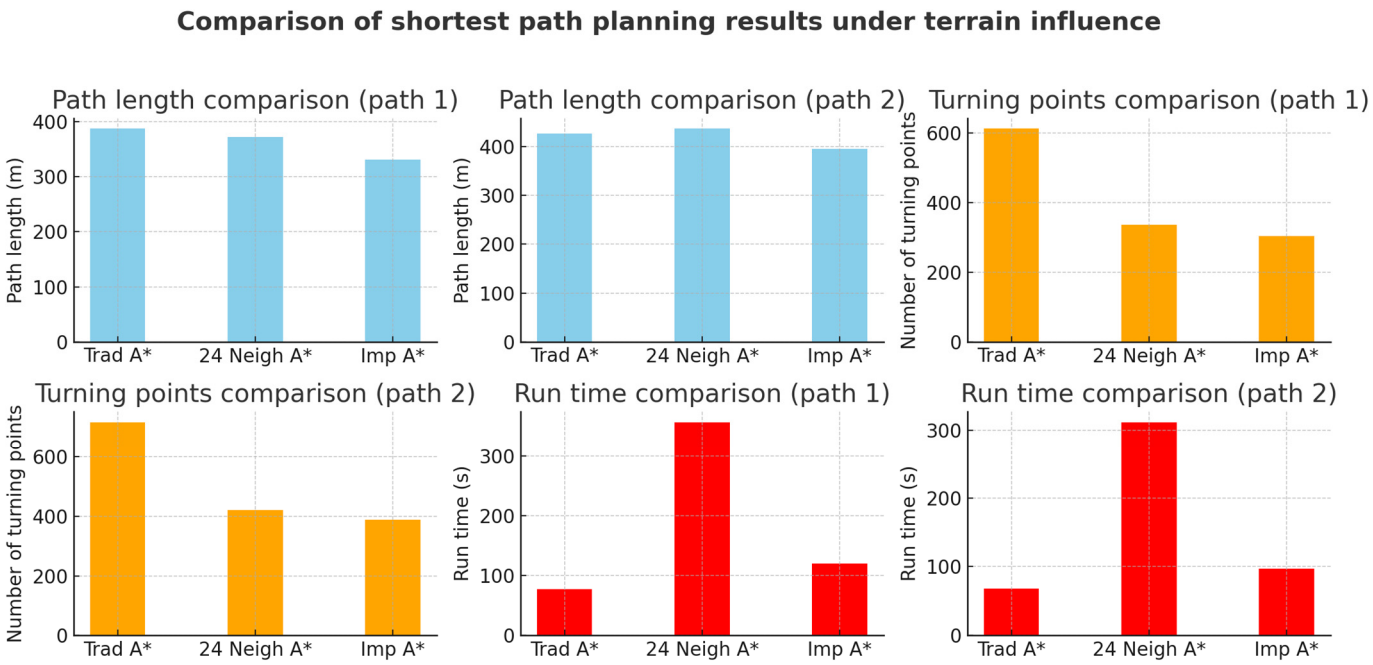


Figure 16. The shortest path planning results obtained under the influence of terrain.

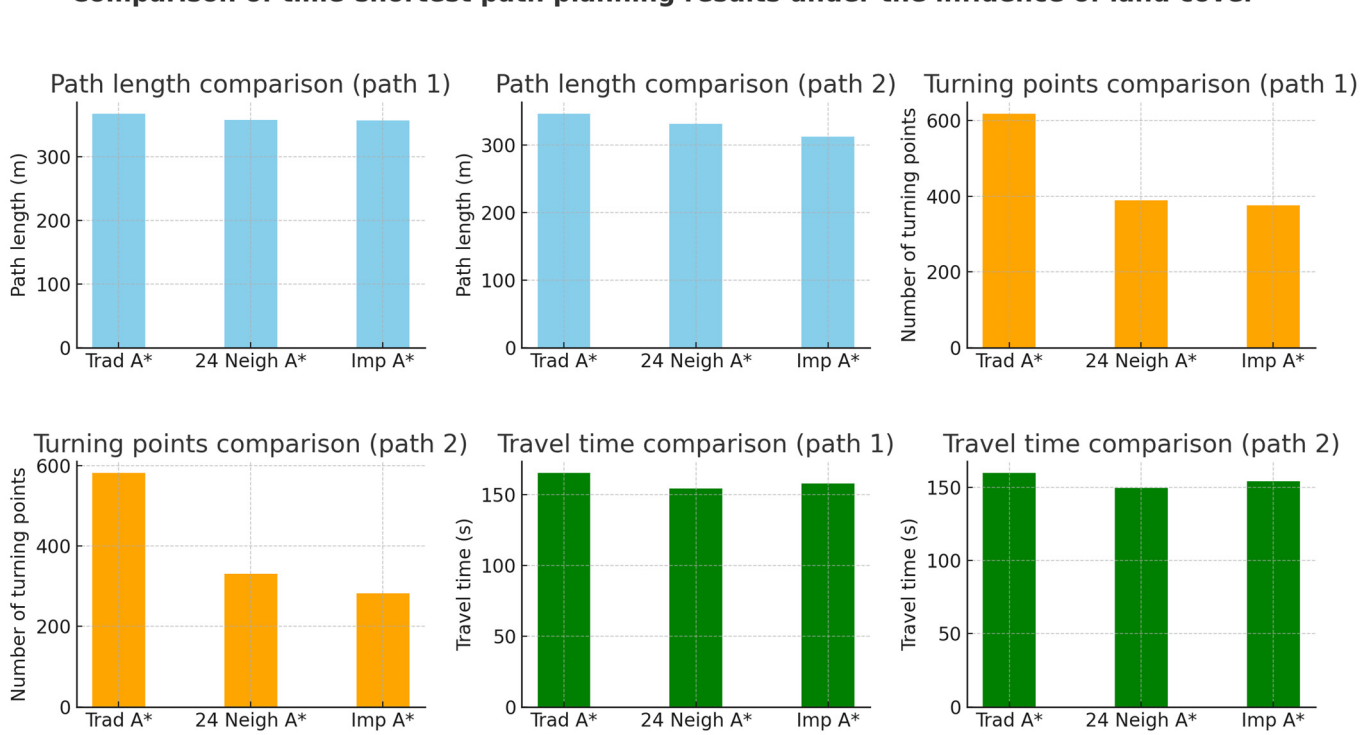


Figure 17. *Cont.*

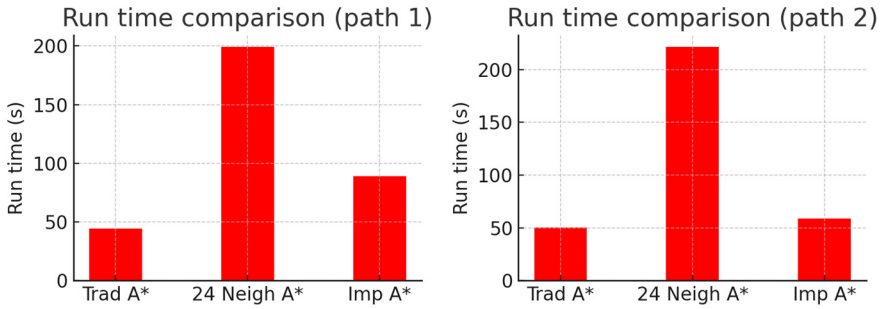


Figure 17. Comparison among the shortest path planning results produced under the influence of land cover.

In the optimal path planning experiment under comprehensive influences, five different algorithms were employed: the traditional 8-neighborhood A* algorithm, the 24-neighborhood A* algorithm, the multi-directional search A* algorithm, the ENMSA-A* algorithm, and the proposed improved A* algorithm. The experimental results are shown in Figure 18. From the figure, it can be observed that the traditional 8-neighborhood A* algorithm performs the worst in optimizing the number of turning points, but it has the shortest running time due to its smaller search range and faster processing speed. In contrast, the multi-directional search A* algorithm performs the best in optimizing the number of turning points, although its running speed is slower. The proposed improved A* algorithm demonstrates excellent performance in terms of path length and traversal speed compared to the other four algorithms. The simulation results indicate that the proposed improved A* algorithm has promising application potential in complex off-road scenarios. Traditional A* algorithms are mostly used in two-dimensional planes. This paper extends the A* algorithm to three-dimensional planes for experimental purposes. In a field environment, many factors need to be considered. If various factors are simply superimposed, the obtained effect may not meet expectations. Therefore, this paper fits the speed curve through the speeds observed under different field conditions, determines the comprehensive influence of the slope and land cover type on the speed, and verifies the results of the experiments.

This paper investigates vehicle navigation in complex field environments and conducts simulation experiments based on the influences of the slope and land cover type on vehicle driving speed. However, this study still has some limitations. First, due to the high precision required for the experimental data, obtaining the data is quite challenging. Additionally, conducting experiments to measure the impact of a 3D environment on vehicle speed incurs significant costs. Furthermore, because the algorithm employs a step-by-step search method between grids, its efficiency may be noticeably reduced when using large-area maps.

Although this study has validated the effectiveness of the improved algorithm through simulation experiments, real-world situations may present additional complexities and uncertainties. Therefore, future work will involve testing in actual scenarios to further enhance the robustness of the improved algorithm through empirical validation. Simultaneously, efforts will be made to optimize the data structures to improve the algorithm's search efficiency, addressing the needs of off-road path planning in large-scale environments. Furthermore, the influence of weather conditions on path planning results will be investigated, as the complex and variable nature of weather significantly impacts off-road driving. This will ensure that the algorithm is applicable to various outdoor driving activities, thereby guaranteeing the safety and efficiency of off-road travel.

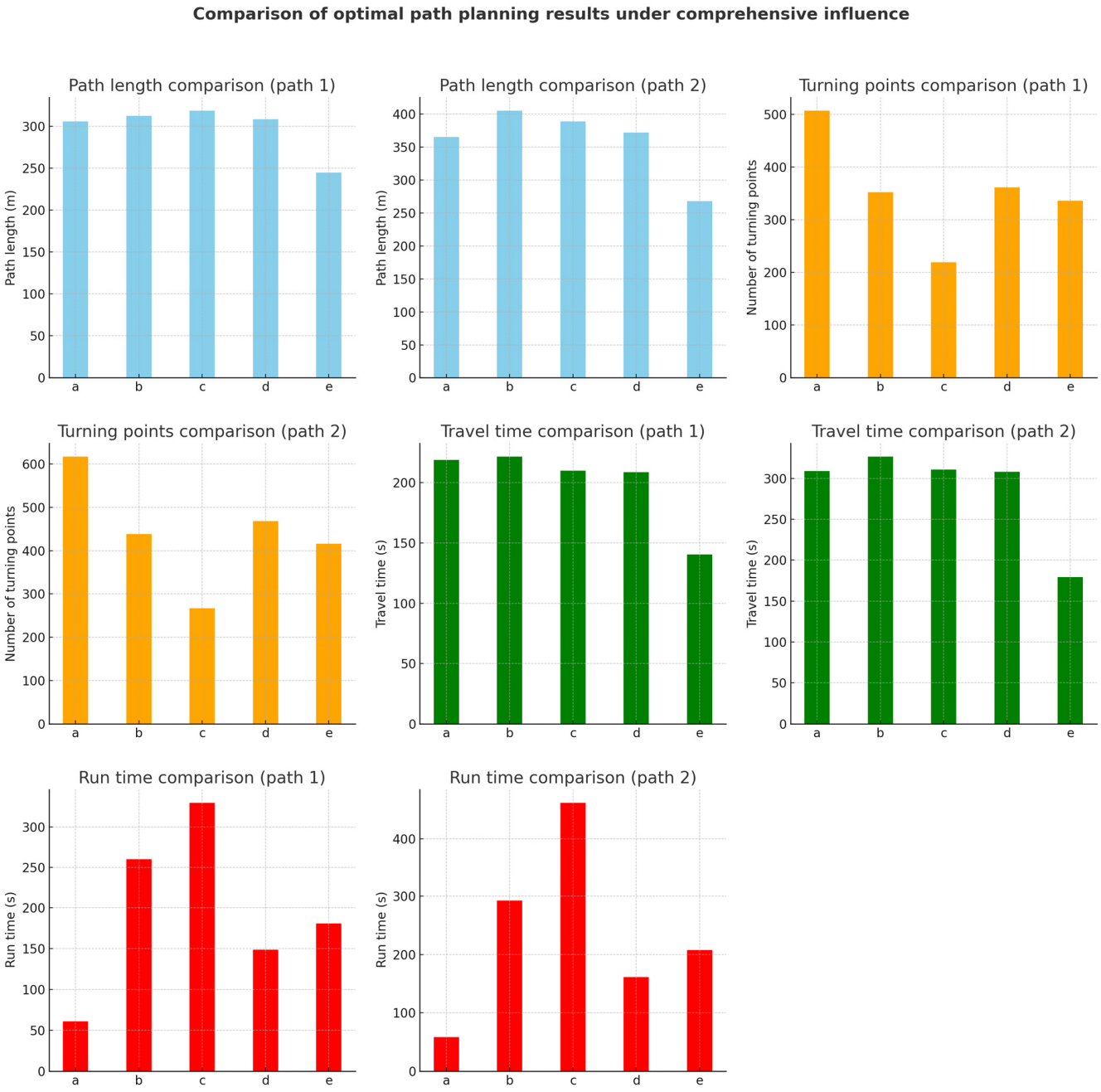


Figure 18. Comparison of optimal path planning results under comprehensive influences: a is traditional A* algorithm; b is 24 search neighborhood A* algorithm; c is multi-direction search algorithm; d is ENMSA-A* algorithm; e is improved algorithm.

6. Conclusions

To solve the many path turning points and poor path results yielded by the traditional A* algorithm, an improved A* algorithm is proposed, and global path planning results are presented for complex wild cases. The improved algorithm adds a linear judgment regarding the comprehensive influence of the slope and land cover to the evaluation function, producing a better effect than that of the traditional superposition judgment; uses an improved dynamic 14-neighborhood search instead of the 8-domain search method of the traditional A* algorithm, which efficiently decreases the number of turning points encountered along the path; and adds obstacle avoidance and corner limiting functions. Three different scenarios were designed to test the functionality of the improved algorithm, and the improved algorithm reduced the path length by 23.30% relative to the results of the

traditional algorithm. The count of turning points reduced by 33.16%, and the travel time decreased by 38.92%. The results showed that the improved algorithm used shorter travel times and shorter path lengths, and the count of turning points was effectively improved. The developed algorithm can be used for navigation in complex field activities such as ecotourism and field geological exploration, thus ensuring the passability and efficiency of the output path planning results.

Author Contributions: Conceptualization, Zhihong Lv and Qing Zhang; methodology, Zhihong Lv; software, Zhihong Lv; validation, Zhihong Lv, Guangjun Qu and Dequan Zhao; formal analysis, Zhihong Lv, Hongchun Peng, Kefa Zhou, Li Ni and Qing Zhang; investigation, Dequan Zhao and Guangjun Qu; resources, Zhihong Lv and Dequan Zhao; data curation, Zhihong Lv, Weiting Yuan and Yue Gao; writing—original draft preparation, Zhihong Lv; writing—review and editing, Zhihong Lv, Hongchun Peng and Qing Zhang; visualization, Zhihong Lv; supervision, Hongchun Peng, Li Ni and Qing Zhang; project administration, Zhihong Lv and Qing Zhang; funding acquisition, Qing Zhang. All authors have read and agreed to the published version of the manuscript.

Funding: This research was funded by the Identification and digital mapping of physical properties of the Martian surface (E2C1051700) and Strategic Priority Research Program of the Chinese Academy of Sciences (Class A) (XDA0430103).

Data Availability Statement: The data presented in this study are available upon reasonable request from the corresponding author.

Conflicts of Interest: The authors declare no conflicts of interest.

References

1. Ma, B.; Liu, Q.; Jiang, Z.; Che, D.; Qiu, K.; Shang, X. Energy-Efficient 3D Path Planning for Complex Field Scenes Using the Digital Model with Landcover and Terrain. *ISPRS Int. J. Geo-Inf.* **2023**, *12*, 82. [CrossRef]
2. Neydorf, R.; Yarakhmedov, O.; Polyakh, V.; Chernogorov, I.; Vucinic, D. Robot Path Planning Based on Ant Colony Optimization Algorithm for Environments with Obstacles. In *Improved Performance of Materials*; Advanced Structured Materials; Springer: Berlin/Heidelberg, Germany, 2018; pp. 175–184.
3. Cao, J. Robot Global Path Planning Based on an Improved Ant Colony Algorithm. *J. Comput. Commun.* **2016**, *4*, 11–19. [CrossRef]
4. Dijkstra, E.W. A note on two problems in connexion with graphs. *Numer. Math.* **1959**, *1*, 269–271. [CrossRef]
5. Chen, Y.-z.; Shen, S.-f.; Chen, T.; Yang, R. Path Optimization Study for Vehicles Evacuation based on Dijkstra Algorithm. *Procedia Eng.* **2014**, *71*, 159–165. [CrossRef]
6. Zhou, X.; Yan, J.; Yan, M.; Mao, K.; Yang, R.; Liu, W. Path Planning of Rail-Mounted Logistics Robots Based on the Improved Dijkstra Algorithm. *Appl. Sci.* **2023**, *13*, 9955. [CrossRef]
7. Hart, P.E.; Nilsson, N.J.; Raphael, B. A formal basis for the heuristic determination of minimum cost paths. *IEEE Trans. Syst. Sci. Cybern.* **1968**, *4*, 100–107. [CrossRef]
8. Wang, C.; Wang, L.; Qin, J.; Wu, Z.; Duan, L.; Li, Z.; Cao, M.; Ou, X.; Su, X.; Li, W. Path planning of automated guided vehicles based on improved A-Star algorithm. In Proceedings of the 2015 IEEE International Conference on Information and Automation, Lijiang, China, 8–10 August 2015; pp. 2071–2076.
9. Xu, H.; Yu, G.; Wang, Y.; Zhao, X.; Chen, Y.; Liu, J. Path Planning of Mecanum Wheel Chassis Based on Improved A* Algorithm. *Electronics* **2023**, *12*, 1754. [CrossRef]
10. Cipriani, G.; Bottin, M.; Rosati, G.; Faccio, M. A Radial Basis Functions approach to collision avoidance in collaborative tasks. *IFAC-Pap.* **2022**, *55*, 307–312. [CrossRef]
11. Fan, X.; Guo, Y.; Liu, H.; Wei, B.; Lyu, W. Improved Artificial Potential Field Method Applied for AUV Path Planning. *Math. Probl. Eng.* **2020**, *2020*, 6523158. [CrossRef]
12. Zong, C.; Han, X.; Zhang, D.; Liu, Y.; Zhao, W.; Sun, M. Research on local path planning based on improved RRT algorithm. *Proc. Inst. Mech. Eng. Part D J. Automob. Eng.* **2021**, *235*, 2086–2100. [CrossRef]
13. Qureshi, A.H.; Ayaz, Y. Intelligent bidirectional rapidly-exploring random trees for optimal motion planning in complex cluttered environments. *Robot. Auton. Syst.* **2015**, *68*, 1–11. [CrossRef]
14. Pérez-Hurtado, I.; Martínez-del-Amor, M.Á.; Zhang, G.; Neri, F.; Pérez-Jiménez, M.J. A membrane parallel rapidly-exploring random tree algorithm for robotic motion planning. *Integr. Comput.-Aided Eng.* **2020**, *27*, 121–138. [CrossRef]
15. Katoch, S.; Chauhan, S.S.; Kumar, V. A review on genetic algorithm: Past, present, and future. *Multimed. Tools Appl.* **2021**, *80*, 8091–8126. [CrossRef]
16. Elhoseny, M.; Tharwat, A.; Hassanien, A.E. Bezier Curve Based Path Planning in a Dynamic Field using Modified Genetic Algorithm. *J. Comput. Sci.* **2018**, *25*, 339–350. [CrossRef]
17. Bakdi, A.; Hentout, A.; Boutami, H.; Maoudj, A.; Hachour, O.; Bouzouia, B. Optimal path planning and execution for mobile robots using genetic algorithm and adaptive fuzzy-logic control. *Robot. Auton. Syst.* **2017**, *89*, 95–109. [CrossRef]

18. Chen, G.; Liu, J. Mobile Robot Path Planning Using Ant Colony Algorithm and Improved Potential Field Method. *Comput. Intell. Neurosci.* **2019**, *2019*, 1932812. [CrossRef]
19. Nie, Z.; Zhao, H. Research on robot path planning based on Dijkstra and Ant colony optimization. In Proceedings of the 2019 International Conference on Intelligent Informatics and Biomedical Sciences (ICIIBMS), Shanghai, China, 21–24 November 2019; pp. 222–226.
20. Xu, G.; Cui, Q.; Shi, X.; Ge, H.; Zhan, Z.-H.; Lee, H.P.; Liang, Y.; Tai, R.; Wu, C. Particle swarm optimization based on dimensional learning strategy. *Swarm Evol. Comput.* **2019**, *45*, 33–51. [CrossRef]
21. Zhang, X.; Lin, Q. Three-learning strategy particle swarm algorithm for global optimization problems. *Inf. Sci.* **2022**, *593*, 289–313. [CrossRef]
22. Bonyadi, M.R.; Michalewicz, Z.J.E.c. Particle swarm optimization for single objective continuous space problems: A review. *Evol. Comput.* 2017; 25, 1–54. [CrossRef]
23. Sung, I.; Choi, B.; Nielsen, P. On the training of a neural network for online path planning with offline path planning algorithms. *Int. J. Inf. Manag.* **2021**, *57*, 102142. [CrossRef]
24. Wu, K.; Abolfazli Esfahani, M.; Yuan, S.; Wang, H. TDPP-Net: Achieving three-dimensional path planning via a deep neural network architecture. *Neurocomputing* **2019**, *357*, 151–162. [CrossRef]
25. Zhou, C.; Huang, B.; Fränti, P. A review of motion planning algorithms for intelligent robots. *J. Intell. Manuf.* **2021**, *33*, 387–424. [CrossRef]
26. Lin, S.; Liu, A.; Wang, J.; Kong, X. A Review of Path-Planning Approaches for Multiple Mobile Robots. *Machines* **2022**, *10*, 773. [CrossRef]
27. Gong, Y.-J.; Li, J.-J.; Zhou, Y.; Li, Y.; Chung, H.S.-H.; Shi, Y.-H.; Zhang, J. Genetic Learning Particle Swarm Optimization. *IEEE Trans. Cybern.* **2016**, *46*, 2277–2290. [CrossRef] [PubMed]
28. Derrac, J.; García, S.; Molina, D.; Herrera, F. A practical tutorial on the use of nonparametric statistical tests as a methodology for comparing evolutionary and swarm intelligence algorithms. *Swarm Evol. Comput.* **2011**, *1*, 3–18. [CrossRef]
29. Heidari, A.A.; Mirjalili, S.; Faris, H.; Aljarah, I.; Mafarja, M.; Chen, H. Harris hawks optimization: Algorithm and applications. *Future Gener. Comput. Syst.* **2019**, *97*, 849–872. [CrossRef]
30. Coello, C.A.C.; Pulido, G.T.; Lechuga, M.S. Handling multiple objectives with particle swarm optimization. *IEEE Trans. Evol. Comput.* **2004**, *8*, 256–279. [CrossRef]
31. Zhan, Z.H.; Zhang, J.; Li, Y.; Chung, H.S. Adaptive particle swarm optimization. *IEEE Trans. Syst. Man Cybern. B Cybern.* **2009**, *39*, 1362–1381. [CrossRef]
32. Karaman, S.; Frazzoli, E. Sampling-based algorithms for optimal motion planning. *Int. J. Robot. Res.* **2011**, *30*, 846–894. [CrossRef]
33. Qureshi, A.H.; Mumtaz, S.; Ayaz, Y.; Hasan, O.; Muhammad, M.S.; Mahmood, M.T. Triangular Geometrized Sampling Heuristics for Fast Optimal Motion Planning. *Int. J. Adv. Robot. Syst.* **2015**, *12*, 10. [CrossRef]
34. Wu, Z.; Meng, Z.; Zhao, W.; Wu, Z. Fast-RRT: A RRT-Based Optimal Path Finding Method. *Appl. Sci.* **2021**, *11*, 11777. [CrossRef]
35. Wang, N.; Wang, T.; Zhang, Z.; Shao, S.; Jiang, Y.; Li, Y. Mobile Robot Path Planning Method Based on an Improved A* Algorithm. In Proceedings of the 2022 12th International Conference on CYBER Technology in Automation, Control, and Intelligent Systems (CYBER), Changbai Mountain, China, 27–31 July 2022; pp. 140–143.
36. Niu, C.; Li, A.; Huang, X.; Li, W.; Xu, C.; Jin, X. Research on Global Dynamic Path Planning Method Based on Improved A* Algorithm. *Math. Probl. Eng.* **2021**, *2021*, 4977041. [CrossRef]
37. Hong, Z.; Sun, P.; Tong, X.; Pan, H.; Zhou, R.; Zhang, Y.; Han, Y.; Wang, J.; Yang, S.; Xu, L. Improved A-Star Algorithm for Long-Distance Off-Road Path Planning Using Terrain Data Map. *ISPRS Int. J. Geo-Inf.* **2021**, *10*, 785. [CrossRef]
38. Bai, J.H.; Oh, Y.-J. Global Path Planning of Lunar Rover Under Static and Dynamic Constraints. *Int. J. Aeronaut. Space Sci.* **2020**, *21*, 1105–1113. [CrossRef]
39. Yu, Z.S. *Theory of Automobiles*, 2nd ed.; China Machine Press: Beijing, China, 2018.
40. Xia, Q.; Tang, Q.; Zhang, L. Quasi three dimensional robot path planning of the improved ant colony algorithm. *Mod. Manuf. Eng.* **2018**, *451*, 59. [CrossRef]
41. Xu, P.; Ding, L.; Gao, H.; Zhou, R.; Li, N.; Deng, Z. Environmental Characterization and Path Planning for Legged Robots Considering Foot-terrain Interaction. *J. Mech. Eng.* **2020**, *56*, 21–33. [CrossRef]
42. Li, X.; Sun, M.; Li, X.; Ren, X. Terrain Traversability Analysis Method for Air-Ground Col- laborative Emergency. *J. Shihezi Univ. (Nat. Sci.)* **2019**, *37*, 12–20. [CrossRef]
43. Song, R.; Liu, Y.; Bucknall, R. Smoothed A* algorithm for practical unmanned surface vehicle path planning. *Appl. Ocean Res.* **2019**, *83*, 9–20. [CrossRef]
44. Fu, B.; Chen, L.; Zhou, Y.; Zheng, D.; Wei, Z.; Dai, J.; Pan, H. An improved A* algorithm for the industrial robot path planning with high success rate and short length. *Robot. Auton. Syst.* **2018**, *106*, 26–37. [CrossRef]
45. Xie, G.; Fang, L.; Su, X.; Guo, D.; Qi, Z.; Li, Y.; Che, J. A Path-Planning Approach for an Unmanned Vehicle in an Off-Road Environment Based on an Improved A* Algorithm. *World Electr. Veh. J.* **2024**, *15*, 234. [CrossRef]
46. You, Z.; Shen, K.; Huang, T.; Liu, Y.; Zhang, X. Application of A* Algorithm Based on Extended Neighborhood Priority Search in Multi-Scenario Maps. *Electronics* **2023**, *12*, 1004. [CrossRef]

Disclaimer/Publisher's Note: The statements, opinions and data contained in all publications are solely those of the individual author(s) and contributor(s) and not of MDPI and/or the editor(s). MDPI and/or the editor(s) disclaim responsibility for any injury to people or property resulting from any ideas, methods, instructions or products referred to in the content.